Molecular basis for allosteric regulation of the type 2 ryanodine receptor channel gating by key modulators

Ximin Chi[a,1], Deshun Gong[a,1,2], Kang Ren[b], Gewei Zhou[b], Gaoxingyu Huang[b], Jianlin Lei[c], Qiang Zhou[a], and Nieng Yan[d,2]

[a]Key Laboratory of Structural Biology of Zhejiang Province, School of Life Sciences, Westlake University, Hangzhou 310024, China; [b]Beijing Advanced Innovation Center for Structural Biology, Tsinghua-Peking Joint Center for Life Sciences, School of Life Sciences, Tsinghua University, Beijing 100084, China; [c]Technology Center for Protein Sciences, Ministry of Education Key Laboratory of Protein Sciences, School of Life Sciences, Tsinghua University, Beijing 100084, China; and [d]Department of Molecular Biology, Princeton University, Princeton, NJ 08544

Contributed by Nieng Yan, October 28, 2019 (sent for review August 20, 2019; reviewed by Liang Feng and Filip L. A. Van Petegem)

The type 2 ryanodine receptor (RyR2) is responsible for releasing Ca^{2+} from the sarcoplasmic reticulum of cardiomyocytes, subsequently leading to muscle contraction. Here, we report 4 cryo-electron microscopy (cryo-EM) structures of porcine RyR2 bound to distinct modulators that, together with our published structures, provide mechanistic insight into RyR2 regulation. Ca^{2+} alone induces a contraction of the central domain that facilitates the dilation of the S6 bundle but is insufficient to open the pore. The small-molecule agonist PCB95 helps Ca^{2+} to overcome the barrier for opening. FKBP12.6 induces a relaxation of the central domain that decouples it from the S6 bundle, stabilizing RyR2 in a closed state even in the presence of Ca^{2+} and PCB95. Although the channel is open when PCB95 is replaced by caffeine and adenosine 5′-triphosphate (ATP), neither of the modulators alone can sufficiently counter the antagonistic effect to open the channel. Our study marks an important step toward mechanistic understanding of the sophisticated regulation of this key channel whose aberrant activity engenders life-threatening cardiac disorders.

type 2 ryanodine receptor | cryo-EM structures | modulators | allosteric regulation

The type 2 ryanodine receptor (RyR2), a calcium (Ca^{2+}) channel expressed in the sarcoplasmic reticulum (SR) membrane of cardiac myocytes, is responsible for releasing Ca^{2+} from the SR into the cytoplasm during excitation–contraction coupling (ECC) (1–3). Physiologically, the opening of the channel occurs in response to Ca^{2+} entry into the cell mediated by the L-type voltage-gated Ca^{2+} channel ($Ca_v1.2$), in a process commonly known as calcium-induced calcium release (CICR) (4–7). RyR2-mediated Ca^{2+} release is fundamental to a number of biological processes, ranging from muscle contraction to learning and memory (8, 9). Aberrations in RyR2 function have been implicated in the pathology of multiple severe diseases. More than 150 mutations in RyR2 are potentially linked to catecholaminergic polymorphic ventricular tachycardia type 1, arrhythmogenic right ventricular dysplasia type 2, and idiopathic ventricular fibrillation (10–16).

Owing to its importance for each heartbeat, RyR2 is subject to sophisticated regulation by a large number of modulators, including ions, particularly Ca^{2+} and Mg^{2+} (17–21); small molecules, such as adenosine 5′-triphosphate (ATP) and caffeine (19, 22–25); and proteins, such as FK506-binding protein 12 and 12.6 (FKBP12/12.6) and calmodulin (CaM) (26–31). During ECC, RyR2 is activated through the CICR mechanism, whereas the skeletal muscle–specific subtype RyR1 is activated by mechanical coupling to $Ca_v1.1$. Although both RyR1 and RyR2 exhibit a biphasic dependence on cytosolic Ca^{2+} concentration (i.e., are activated by micromolar level of Ca^{2+} and inhibited by millimolar level of Ca^{2+}), RyR2 is activated to a greater extent by cytosolic Ca^{2+} and requires higher [Ca^{2+}] for inhibition in the absence of other activators (32), indicating important differences between these 2 RyR isoforms with respect to their activation and inhibition by Ca^{2+}.

FKBP12.6 is one of the most prominent RyR2-binding proteins. Although the effect of FKBP12.6 on RyR2 has been extensively studied, the precise role of FKBP12.6 in regulating the channel is still controversial. Marks and coworkers found that FKB12.6 stabilizes RyR2 in a closed state to prevent the leakage of SR Ca^{2+} into the cytoplasm, and the dissociation of FKBP12.6 from RyR2 leads to SR Ca^{2+} leakage, which ultimately impairs contractility and promotes arrhythmia (27, 31, 33, 34). However, contradictory findings have been reported by other groups, raising the question of whether FKBP12.6 plays pathophysiological roles in heart failure. One study showed that neither FKBP12.6 nor FKBP12 affects RyR2 function (35, 36). Another study suggested that FKBP12 could activate RyR2 and FKBP12.6 might act as an antagonist to FKBP12 without directly lowering the open probability (Po) of RyR2 (37). To make the functional roles of FKBPs in RyR2 function more perplexing, a recent report suggested that both FKBP12.6 and FKBP12 play critical roles in regulating RyR2 function by facilitating the termination of spontaneous Ca^{2+} release or store overload-induced Ca^{2+} release, providing another mechanism for the regulation of RyR2 by FKBP12.6 (38).

Significance

As a switch for the release of Ca^{2+} from the sarco(endo)plasmic reticulum of cardiomyocytes, the type 2 ryanodine receptor (RyR2) is subject to sophisticated regulation by a broad spectrum of modulators. Dysregulation of RyR2-mediated Ca^{2+} release is linked to life-threatening cardiac arrhythmias. The regulatory mechanism of RyR2 by key modulators, such as Ca^{2+}, FKBP12.6, ATP, and caffeine, remains unclear. This study provides important insights into the long-range allosteric regulation of RyR2 channel gating by these modulators and serves as an important framework for mechanistic understanding of the regulation of this key player in the excitation–contraction coupling of cardiac muscles.

Author contributions: D.G. and N.Y. designed research; X.C., D.G., K.R., G.Z., G.H., J.L., and Q.Z. performed research; X.C., D.G., K.R., G.Z., G.H., J.L., Q.Z., and N.Y. analyzed data; and D.G. and N.Y. wrote the paper.

Reviewers: L.F., Stanford University; and F.L.A.V.P., University of British Columbia.

The authors declare no competing interest.

Data deposition: Atomic coordinates and EM density maps of Ca^{2+} alone (PDB ID code 6JG3; EMDB ID code EMD-9823), F/P/Ca^{2+} (PDB ID code 6JGZ; EMDB ID code EMD-9824), F/A/Ca^{2+} (PDB ID code 6JH6; EMDB ID code EMD-9825), and F/C/Ca^{2+} (PDB ID code 6JHN; EMDB ID code EMD-9826) have been deposited in the Protein Data Bank (PDB), http://www.rcsb.org, and the Electron Microscopy Data Bank (EMD), https://www.ebi.ac.uk/pdbe/emdb/.

[1]X.C. and D.G. contributed equally to this work.

[2]To whom correspondence may be addressed. Email: gongdeshun@westlake.edu.cn or nyan@princeton.edu.

This article contains supporting information online at https://www.pnas.org/lookup/suppl/doi:10.1073/pnas.1914451116/-/DCSupplemental.

First published December 2, 2019.

Therefore, the pathophysiological roles of FKBP12.6 in the regulation of RyR2 need to be further investigated.

Single-channel studies reported that cytosolic Ca^{2+} alone is a poor activator of RyRs and does not increase Po above 0.5 in the absence of other activating ligands. The presence of micromolar cytosolic Ca^{2+}, plus a second ligand, is required for full activation of the channel (20, 22, 39, 40). ATP is a well-known physiological agonist likely to be constitutively bound to RyR2 since the cellular ATP concentration is at millimolar levels in cardiac cells (22). Caffeine has long been used as a pharmacological probe for investigating RyR-mediated Ca^{2+} release and cardiac arrhythmias (41, 42), and 2,2′,3,5′,6-pentachlorobiphenyl (PCB95) also activates RyRs (43–45).

Structures of RyR2 in the open state have been captured in the presence of PCB95/Ca^{2+} without FKBP12.6 (denoted P/Ca^{2+}) (46) and in the presence of ATP/caffeine/Ca^{2+} with FKBP12.6 (47) (denoted F/A/C/Ca^{2+}). The latter revealed that Ca^{2+}, ATP, and caffeine are all located at the interfaces between the central and channel domains, identical to those in the structures of RyR1 (48). However, the regulation of RyR2 gating by each individual modulator alone requires further dissection through comparative structural studies.

To address these questions, we hereby report 4 cryo-electron microscopy (cryo-EM) structures of porcine RyR2 bound to distinct modulators, which together with our published structures (46, 47), provide important insight into the long-range allosteric regulation of RyR2 channel gating by these key modulators.

Results

Structure Determination of RyR2 in Multiple Functional States. Based on our published structures of closed RyR2 in 5 mM ethylenediaminetetraacetic acid (EDTA) (denoted apo-RyR2), open RyR2 in the presence of 20 μM Ca^{2+} and 10 μM PCB95 (denoted P/Ca^{2+}) (46), and open RyR2-FKBP12.6 complex in the presence of 20 μM Ca^{2+}, 5 mM ATP, and 5 mM caffeine (denoted F/A/C/Ca^{2+}) (47), we determined the cryo-EM structures of RyR2 under 4 additional conditions: 1) Ca^{2+} alone at 20 μM (denoted Ca^{2+} alone) at 6.1 Å, 2) Ca^{2+} plus 10 μM PCB95 and FKBP12.6 (denoted F/P/Ca^{2+}) at 4.6 Å, 3) Ca^{2+} plus FKBP12.6 and 5 mM ATP (denoted F/A/Ca^{2+}) at 4.8 Å, and 4) Ca^{2+} plus FKBP12.6 and 5 mM caffeine (denoted F/C/Ca^{2+}) at 4.5 Å (*SI Appendix*, Figs. S1–S3). The conditions for each dataset are summarized in *SI Appendix*, Table S1. Condition 1 was used to investigate the mechanisms of the allosteric regulation of RyR2 channel gating by Ca^{2+} and PCB95. Condition 2 was used to investigate the mechanisms of the long-range allosteric regulation of RyR2 channel gating by FKBP12.6. Conditions 3 and 4 were used to investigate the stimulatory mechanisms of RyR2 by caffeine and ATP.

Previously, we purified RyR2 using glutathione *S*-transferase (GST)-fused FKBP12 as bait and found that the RyR2/GST-FKBP12 complex fell apart during size exclusion chromatography (SEC) purification (46). In this study, the proteins under conditions that included FKBP12.6 were purified using GST-FKBP12.6 as bait. The RyR2/GST-FKBP12.6 complex survived during SEC (*SI Appendix*, Fig. S1*A*), indicating that RyR2 has a higher binding affinity for FKBP12.6 than for FKBP12.

All cryo-EM datasets were processed with the same procedure (*SI Appendix*, Figs. S2 and S3). For all of the structures, the resolution of the peripheral structures, such as P1, P2, HD2, the 3 SPRY domains, and the NTD subdomains NTD-A/B, which are rich in β-strands, is insufficient for detailed analysis, whereas the secondary structural elements of other domains are well resolved. To describe the intricate conformational changes, the RyR2 structure with resolved secondary structural elements is divided into 3 layers: the channel domain as layer 1, the central domain as layer 2, and the peripheral region containing the NTD-C, HD1, and handle domains as layer 3 (Fig. 1*A*).

It is noted that lipids were reported to affect the Po of RyR1 (49). Therefore, conclusions reported in this study, wherein the detergent digitonin was used for all conditions, may be subject to modification. Furthermore, it is unpractical to estimate the precise concentration of Ca^{2+} applied to RyR2 during cryosample preparation because of the high concentrations of Ca^{2+} present in the blotting paper (50). Consequently, the related analysis pertains to relative differences.

PCB95 Helps Ca^{2+} to Overcome the Barrier for Opening RyR2. It has been shown that Ca^{2+} alone did not yield structures of open RyR1 under detergent conditions (48). In contrast to activation of RyR1 by direct physical contact with $Ca_v1.1$, Ca^{2+} serves as the signaling trigger for RyR2 activation. To investigate whether Ca^{2+} alone could open the channel without any effect from other modulators under cryoconditions, 20 μM Ca^{2+} was applied to stimulate the channel (46).

The pore constriction site was seen to shift from Ile4868 in the closed apo-RyR2 structure to Gln4864 in the open P/Ca^{2+} structure (46). When the structure of Ca^{2+} alone is superimposed on that of apo-RyR2 relative to the channel domain, all 3 layers tilt outward and clockwise with respect to the vertical axis of the channel (Fig. 1*B* and *SI Appendix*, Fig. S4*A*), but the constriction site residue remains Ile4868 with a distance between the Cα atoms of 11 Å, identical to that in the apo-RyR2 structure (Fig. 1*C*). These results are consistent with the observation in RyR1, wherein Ca^{2+} alone primes RyR2 for opening but additional agonists are required to overcome the barrier to opening (48).

Multiple studies have shown that the central domain serves as the transducer for the long-range allosteric gating of channel opening through coupling between the U-motif of the central domain and the O-ring of the channel domain formed by the C-terminal domain (CTD), the cytoplasmic region in the voltage-sensor-like (VSL) domain (VSC), and the cytoplasmic segment of S6 (S6C) (46, 51, 52). During channel opening, the auxiliary motifs of the central domain, including the preceding helix α0, a capping helix α4, and the U-motif on the C-terminal end, fold toward the center of the concave surface (inward movements) of the central domain (Fig. 1*D*) (46). Ca^{2+} alone induces obvious inward movements of the central domain in these regions, but to a smaller degree (Fig. 1 *D* and *E*). The O-ring of the channel domain and the U-motif of the central domain undergo concordant conformational changes (Fig. 1 *E* and *F*). Due to extensive interactions between the O-ring and U-motif (52), the inward movements of the U-motif, induced by Ca^{2+}, may provide a pulling force to facilitate the S6 bundle dilation. This process is analogous to bow drawing, wherein the central domain represents the bow and Ca^{2+} affords the drawing force (Fig. 1*F* and Movie S1), which is akin to the effect of Ca^{2+} on RyR1 in the 3-[(3-cholamidopropyl) dimethylammonio]-1-propanesulfonate hydrate (CHAPS) plus 1,2-dioleoyl-*sn*-glycerol-3-phosphocholine (DOPC) condition (48) (*SI Appendix*, Fig. S5*A*). We refer to the inward folding of the central domain toward its concave side as contraction and the opposite motion as relaxation.

The interactions between 2 neighboring NTD domains were proposed as an important gating factor (53). Channel opening requires breaking of the interactions along the interface between NTD-A and neighboring NTD-B′ (interface 1) (53). Ca^{2+} alone appears to significantly extend the intersubunit gap between NTD-A and the neighboring NTD-B′ (*SI Appendix*, Fig. S5*B*).

Although no density was observed for PCB95 in the P/Ca^{2+} structure (46), the structure with Ca^{2+} alone, obtained in the present study, demonstrates that PCB95 helps Ca^{2+} to overcome the barrier for opening (Fig. 1 *B–D* and *SI Appendix*, Fig. S4*B*). PCB95 was previously reported to activate RyR1 in an FKBP12-mediated mechanism. The PCB95-enhanced binding of [^{3}H] ryanodine to RyR1 is completely eliminated if the interaction of FKBP12 with RyR1 is disrupted by FK506 or rapamycin (44, 54).

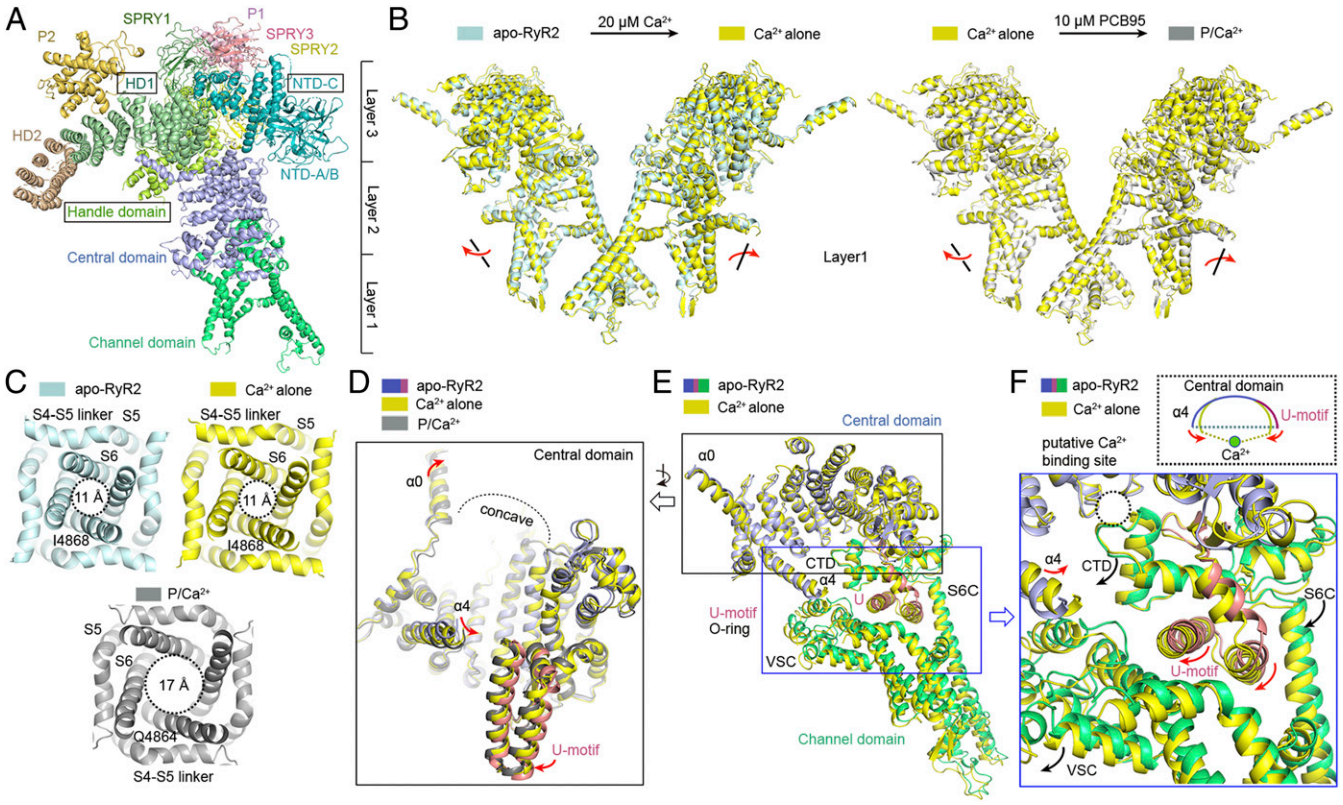

Fig. 1. PCB95 facilitates Ca^{2+} to overcome the barrier in opening the gate of RyR2. (*A*) Domain organization of a RyR2 protomer. To facilitate description of the conformational changes throughout this study, the domains with resolved secondary structure elements are divided into 3 layers from the luminal side to the cytoplasmic side. Layer 1 contains the channel domain. Layer 2 contains the central domain. Layer 3 contains the HD1 and handle domain and NTD-C. (*B*) Ca^{2+} induces conformational changes in the channel domain but is insufficient to open the channel (*Left*). Addition of PCB95 induces further conformational changes that open the channel (*Right*). Shown here are the structural superimpositions between apo-RyR2 and Ca^{2+} alone and between Ca^{2+} alone and P/Ca^{2+} relative to the channel domain. Red arrows indicate the direction of conformational changes. (*C*) The pore remains closed in the presence of 20 μM Ca^{2+} alone. The cytosolic view is shown for RyR2 under the 3 indicated conditions. The indicated distances were measured between the Cα atoms of the Gln4864 (open structure) or Ile4868 (closed structure) gating residue on the S6 segments in the diagonal protomers. (*D*) Intradomain shifts of the central domain among the structures apo-RyR2, RyR2 in the presence of 20 μM Ca^{2+} (Ca^{2+} alone), and RyR2 in the presence of both PCB95 and Ca^{2+} (P/Ca^{2+}). Red arrows indicate the direction of conformational changes. (*E*) The central domains and channel domains of the structures apo-RyR2 and Ca^{2+} alone were superimposed relative to the central domain. (*F*) Ca^{2+} induces a contraction of the central domain that provides a pulling force for facilitating the dilation of the S6 bundle. Red arrows indicate the direction of conformational changes of the U-motif and helix α4. Black arrows indicate the direction of conformational changes of the O-ring, which is formed by the CTD, cytoplasmic subdomain in the VSC, and S6C. All EM maps were generated in Chimera (72). All structure figures were prepared using PyMOL (https://pymol.org/2/).

In contrast to the activation of RyR1 by PCB95, our structures of RyR2, in the absence of FKBP12 or FKBP12.6, indicate that PCB95 can facilitate Ca^{2+} for RyR2 opening, in the absence of FKBP.

FKBP12.6 Stabilizes RyR2 in a Closed State. We attempted to investigate the regulation of FKBP12.6 on RyR2 by controlling a clean background, wherein FKBP12.6 was the only difference between the P/Ca^{2+} and F/P/Ca^{2+} conditions. The FKBP12.6 binding site on RyR2, which is identical to that on RyR1 for FKBP12 and FKBP12.6 (48, 52), is located in the cleft formed by the SPRY1, SPRY3, NTD, and handle domains (Fig. 2*A* and *SI Appendix*, Fig. S6*A*). A hydrophobic loop from the handle domain extends into the ligand-binding pocket of FKBP12.6 (*SI Appendix*, Fig. S6*B*). Compared to the EM map of P/Ca^{2+}, additional density corresponding to HD2 in F/P/Ca^{2+}, similar to that observed in the 11.8 Å resolution EM map of rabbit RyR2 (rRyR2) bound to FKBP12.6 (55), was resolved and folds toward the main body of the structure (Fig. 2*B*). In addition, the P2 domain was partially resolved to be in contact with the SPRY3′ domain in the neighboring protomer (Fig. 2*B*). These further resolved densities suggest that the allosteric changes, induced by FKBP12.6, may be transmitted to the P2 and HD2 domains in both the same and neighboring protomers and increase their rigidity. However, the density of HD2 in RyR2 is still partially missing compared to what has been resolved in RyR1 (52), and most of the main chain in HD2 is not traceable even in the presence of FKBP12.6 (*SI Appendix*, Fig. S6 *C* and *D*).

It is noted that HD2 in RyR1 contacts the SPRY2′ domain and is positioned adjacent to the P1′ domain in the neighboring protomer. In contrast, the density of HD2 in RyR2, as well as that in rRyR2 (55), is close to the handle domain in the same protomer and distant from the SPRY2′ and P1′ domains in the neighboring protomer (*SI Appendix*, Fig. S6 *C* and *D*).

Superimposing the P/Ca^{2+} and F/P/Ca^{2+} structures relative to the channel domain shows that FKBP12.6 induces inward and counterclockwise rotation of layers 1 and 2 and outward and counterclockwise rotation of layer 3 (*SI Appendix*, Fig. S7*A*), which significantly shortens the intersubunit gap at interface 1 (*SI Appendix*, Fig. S7*B*). Superimposing the NTD, handle, and central domains of F/P/Ca^{2+} on those of P/Ca^{2+}, relative to the central domain, reveals outward tilt of the NTD and handle domain with respect to the central domain, accompanied by an outward movement of helices α0 and α1 of the central domain due to the interaction between helix α0 and the handle domain (Fig. 2*C*).

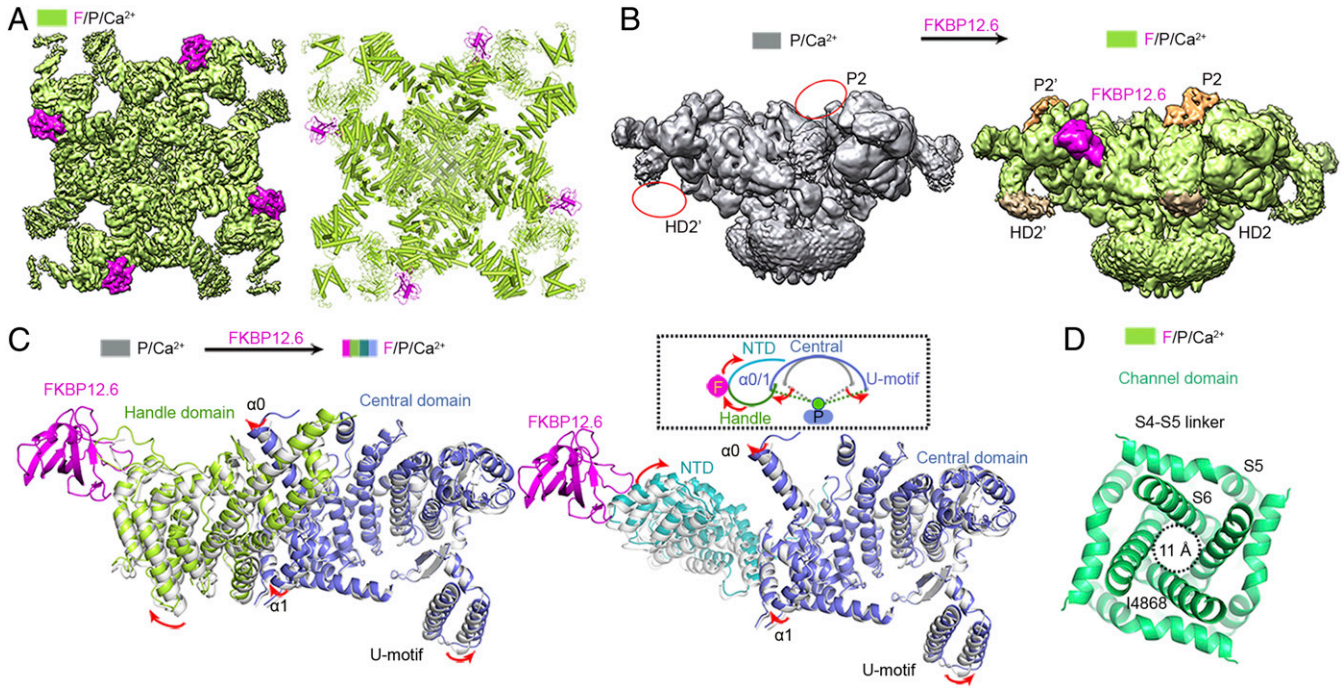

Fig. 2. FKBP12.6 stabilizes RyR2 in a closed state. (*A*) The EM map and atomic model of RyR2 in a complex with FKBP12.6, PCB95, and Ca^{2+} ($F/P/Ca^{2+}$). FKBP12.6 is colored magenta. The map is shown at a contour level of 0.025. (*B*) FKBP12.6 serves as a stabilizer to enhance the rigidity of the HD2 and P2 domains. Shown here are the EM maps (low pass filtered to 6 Å resolution) of the P/Ca^{2+} and $F/P/Ca^{2+}$ structures. Additional density for the HD2 and P2 domains can be resolved in the $F/P/Ca^{2+}$ structure, whereas the corresponding density is absent in the P/Ca^{2+} structure. (*C*) FKBP12.6 induces the NTD and handle domains to tilt outward with respect to the central domain, likely providing a pulling force for relaxing the central domain. The NTD, handle, and central domains of the structures P/Ca^{2+} and $F/P/Ca^{2+}$ were superimposed relative to the central domain. Red arrows indicate the direction of conformational changes. (*D*) The pore is kept closed in the $F/P/Ca^{2+}$ structure. The indicated distances were measured between the Cα atoms of the Ile4868 gating residue on the S6 segments in the diagonal protomers.

The motions of the NTD and handle domains, induced by FKBP12.6, likely provide a pulling force for the central domain, resulting in the outward movement of the U-motif relative to the center of the concave surface (Fig. 2*C* and Movie S2). Consequently, RyR2 is stabilized in a closed state, as evidenced by the shift of the pore constriction site from Gln4864 in the P/Ca^{2+} structure to Ile4868 in the $F/P/Ca^{2+}$ structure with the distance between the Cα atoms of Ile4868 in the diagonal protomers shortened to ∼11 Å (Fig. 2*D*).

The comparative structure analyses indicate that the antagonistic effect of FKBP12.6 overcomes the synergistic activation by Ca^{2+} and PCB95, resulting in RyR2 closure in the detergent-embedding environment.

The Synergistic Effects of ATP/Caffeine/Ca^{2+} Open FKBP12.6-Bound RyR2. Our recent structural study reveals channel opening upon the synergistic activation of RyR2 by ATP/caffeine/Ca^{2+} in the presence of FKBP12.6 (47). To investigate whether all 3 positive modulators are required for channel opening, ATP/Ca^{2+} and caffeine/Ca^{2+} were applied separately to FKBP12.6-bound RyR2. The distances between the Cα atoms of the Ile4868 constriction site residue in the diagonal protomers of both the $F/A/Ca^{2+}$ and $F/C/Ca^{2+}$ structures are ∼11 Å (Fig. 3*A*), indicating that neither ATP/Ca^{2+} nor caffeine/Ca^{2+} is sufficient to activate the channel in the presence of FKBP12.6.

Compared to the $F/A/Ca^{2+}$ structure, caffeine causes expansion throughout the entire RyR2 molecule with respect to the vertical axis of the channel in the $F/A/C/Ca^{2+}$ structure (*SI Appendix*, Fig. S8*A*) and extends the intersubunit gap at interface 1 (*SI Appendix*, Fig. S8*B*). Similarly, ATP also induces all 3 layers to rotate outward and clockwise (*SI Appendix*, Fig. S8*C*) but slightly shortens the intersubunit gap at interface 1 (*SI Appendix*, Fig. S8*D*). Superimposing the channel domains and U-motifs of the $F/A/Ca^{2+}$, $F/C/Ca^{2+}$, and $F/A/C/Ca^{2+}$ structures, relative to the CTD, shows coupled motion between the CTD and the U-motif because there is no relative motion between these 2 domains, an observation consistent with our previous studies (46, 51). Interestingly, ATP and caffeine induce the same direction of conformational changes in the remaining elements of the channel domain, including the VSL, S4–S5 linker, S5, the selectivity filter (SF), and S6 (Fig. 3*B*), reflecting the synergistic effects of ATP and caffeine. It is noted that caffeine/Ca^{2+} facilitates the movement of almost all of the elements of the channel domain, except the S4–S5 linker and CTD, to a position closer to the open state than that of ATP/Ca^{2+} (Fig. 3*B*).

Molecular Basis for the Synergistic Effects of Ca^{2+}, ATP, and Caffeine. Structural studies of RyR1 and RyR2 both reveal that Ca^{2+} is located at a cleft formed by the central domain and CTD; ATP is buried in a pocket formed by the U-motif, S6C, and CTD, and caffeine is located at the interface formed by the U-motif, helix α4, CTD, and VSC (47, 48) (Fig. 3*C*).

To investigate the mechanism for the requirement of synergistic action of ATP/caffeine/Ca^{2+} to open RyR2 in the presence of FKBP12.6, the central domains and S6Cs of the $F/A/Ca^{2+}$, $F/C/Ca^{2+}$, and $F/A/C/Ca^{2+}$ structures were superimposed. Compared to the $F/A/C/Ca^{2+}$ structure, helix α4 and the 2 helices of the U-motif in the $F/A/Ca^{2+}$ structure undergo an outward motion relative to the center of the concave surface (Fig. 3*D*). Interestingly, helix α4 in the helical repeats of the central domain and helix 2 of the U-motif in the $F/C/Ca^{2+}$ structure remain nearly unchanged, indicating that caffeine locks them together to maintain a pulling force that favors dilation of the S6 bundle (Fig. 3*E*). ATP strengthens the effect of caffeine (Fig. 3*E*). These results

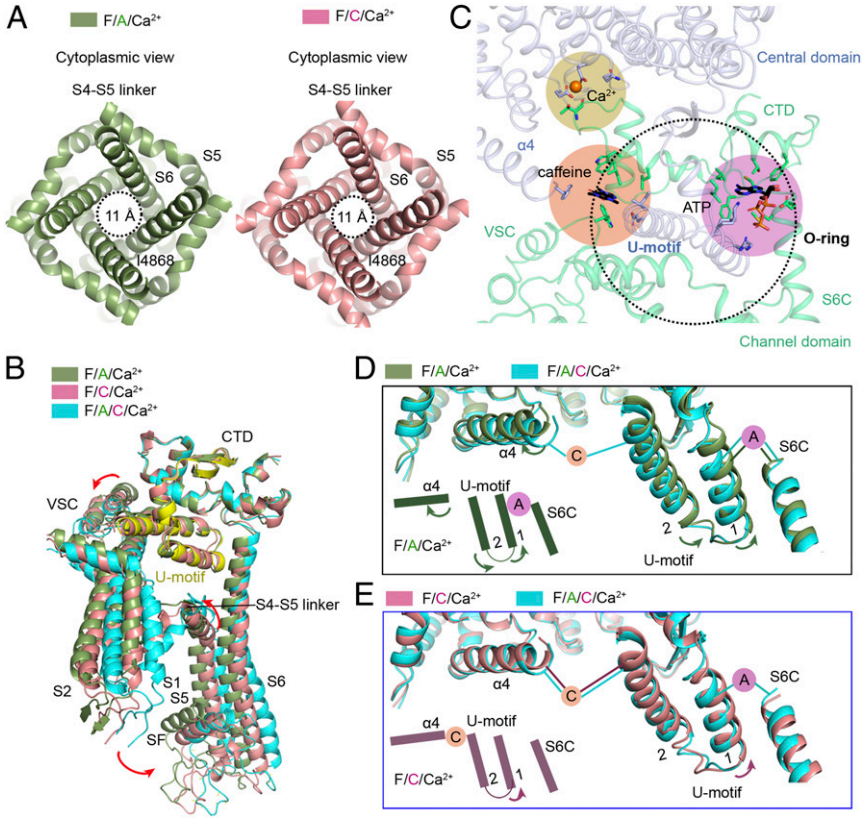

Fig. 3. Molecular basis for the synergistic effects of Ca^{2+}, ATP, and caffeine. (*A*) Neither ATP/Ca^{2+} nor caffeine/Ca^{2+} is sufficient to open the channel in the presence of FKBP12.6. The indicated distances were measured between the Cα atoms of Ile4868 gating residue on the S6 segments in the diagonal protomers. (*B*) The synergistic effects of caffeine and ATP on the channel domain. The structures were superimposed relative to the CTD. (*C*) The binding sites of Ca^{2+}, ATP, and caffeine on RyR2. The dotted circle represents the O-ring that is formed by the CTD, VSC, and S6C. Ca^{2+} is located in the cleft that is formed by the central domain and CTD. ATP is located in a pocket formed by the U-motif, CTD, and S6C. Caffeine is located at the interface formed by the U-motif and helix α4 of the central domain, CTD, and VSC. (*D*) Conformational changes of the central domain induced by caffeine. Shown here are the superimposed structures of F/A/Ca^{2+} and F/A/C/Ca^{2+}. Arrows indicate the direction of conformational changes from the F/A/C/Ca^{2+} to F/A/Ca^{2+} structure. (*E*) Caffeine locks the central domain in a constitutively contracted state, and ATP strengthens the pulling force of caffeine by linking the U-motif and S6. Arrows indicate the direction of conformational changes from the F/A/C/Ca^{2+} to F/C/Ca^{2+} structure.

indicate that ATP and caffeine keep the central domain in a constitutively contracted state, thus stabilizing RyR2 in an open state, even in the presence of FKBP12.6.

Discussion

Although the binding affinity of FKBP12.6 for RyR2 is higher than that of FKBP12 for RyR2, the abundance of FKBP12.6 in cardiac tissue is much lower than that of FKBP12 (56), resulting in only 10 to 20% of endogenous myocyte RyR2 in association with FKBP12.6 (57). In addition, compounds used to dissociate FKBPs from RyRs, such as rapamycin and FK506, were suggested to directly affect the activity of RyRs in an FKBP-independent manner (58, 59). These issues complicate the previous results regarding the functional effects of FKBP12.6 on RyR2 (60). In our present study, FKBP12 was removed by SEC without using macrocyclic lactone ring compounds. Here, the regulatory effect of FKBP12.6 on RyR2 channel gating was examined by comparative structural analyses in a molecular background clearer than in previous functional studies. However, FKBP12.6 and FKBP12 share 85% sequence homology and have similar 3-dimensional (3D) structures (61). The resolved structures cannot offer an explanation of the markedly different affinities of FKBP12.6 and FKBP12 binding to RyR2 because the interface residues are nearly identical between FKBP12 and FKBP12.6 and between RyR1 and RyR2 (46, 62). Among the varied residues between FKBP12 and FKBP12.6, only F59W is located in the ligand-binding pocket of FKBP12.6 (*SI Appendix*, Fig. S9). The basis underlying the markedly different affinities of FKBP12.6 and FKBP12 binding to RyR2 remains to be determined.

The P2 domain is a phosphorylation hot spot, containing a flexible phosphorylation loop (63). Only recently was it reported that the phosphorylation loop, which was invisible in the crystal structure of the P2 domain alone, can wrap around the large lobe of the cAMP-dependent protein kinase A catalytic subunit (PKAc) (64). In addition, phosphorylation can significantly affect affinity and activity of PKA (64). Our structures show that the rigidity of the P2 domain is increased in the presence of FKBP12.6, suggesting a potential correlation between FKBP12.6 and phosphorylation, which awaits further investigation. Furthermore, the contact between the P2 and SPRY3′ domains indicates potential communications between these 2 domains. High-resolution structures of this region are required to elucidate the underlying mechanisms.

The state of RyR2 is defined by the balance of different modulators. Under cryoconditions with rapidly vitrified, detergent-solubilized RyR2, Ca^{2+} alone leads to a rearrangement of the central domain and channel domain that primes RyR2 to open (Fig. 1). Channel opening occurs upon the activation of RyR2 by Ca^{2+} with the help of PCB95 in the absence of FKBP12.6 (46) or with the simultaneous addition of ATP and caffeine in the presence of FKBP12.6 (47); this suggests that the CICR process must

be highly regulated by multiple modulators under physiological conditions.

In summary, 7 different states of RyR2 bound to different combinations of modulators, including our published structures of apo-RyR2 in a closed state and P/Ca^{2+} and F/A/C/Ca^{2+} in open states (46, 47), were compared in detail in this report. These structures collectively provide a mechanistic understanding of the transition from the closed state to the open state regulated by multiple modulators, which marks an important step toward elucidating the complicated regulatory mechanisms of RyR2 (Fig. 4).

The contraction and relaxation of the central domain, which favor the opening and closure of the channel, respectively, are critical for channel gating, confirming the essential role of the central domain in the long-range, allosteric gating of RyRs (51, 52). Under Ca^{2+}-free conditions (apo-RyR2 for the EDTA-treated sample), RyR2 is inactive because of the absence of stimulation by cytoplasmic Ca^{2+}. An increase of [Ca^{2+}] to nominally 20 μM induces a contraction of the central domain, applying a pulling force that facilitates the dilation of the S6 bundle. Addition of PCB95 induces further contraction of the central domain and opens the channel. FKBP12.6 induces relaxation of the central domain, stabilizing RyR2 in a closed state, supporting the pathophysiological regulation of RyR2 by FKBP12.6 (27, 31). Neither Ca^{2+}/ATP nor Ca^{2+}/caffeine is sufficient to open the channel in the presence of FKBP12.6. Caffeine keeps the central domain in a constitutive contraction state, and ATP strengthens the pulling force by bridging the U-motif and S6. The 2 agonistic effects together lead to channel opening (47). It remains to be investigated whether Ca^{2+}/ATP or Ca^{2+}/caffeine can open RyRs in the absence of FKBPs. More importantly, whether conclusions reported for the channels embedded in detergent micelles can be applied to those in a more native environment, such as in a nanodisc, has yet to be investigated.

Materials and Methods

Expression and Purification of GST-FKBP12.6 and GST-FKBP12. Due to the unavailability of porcine FKBP12.6 and FKBP12 sequences in the public domain, human FKBP12.6 and FKBP12 were used for affinity purification of RyR2 from porcine heart (pRyR2) (46). The complementary DNAs of full-length human *FKBP12.6* and *FKBP12* were cloned into the pGEX-4T-2 vector with an N-terminal GST tag and a C-terminal 6xHis tag. The same procedures were used for the expression and purification of FKBP12.6 and FKBP12. In brief, the proteins were expressed in the BL21 (DE3) strain at 18 °C overnight by the addition of 0.2 mM isopropyl -d-1-thiogalactopyranoside (IPTG) to the cells with an optical density at 600 nm (OD_{600}) of 1.0. Cells were collected and resuspended in lysis buffer containing 25 mM tris(hydroxymethyl) aminomethane (Tris), pH 8.0, and 150 mM NaCl. After removing the cell debris by centrifugation at 22,000 × *g* for 1 h, the supernatant was applied to Ni^{2+}-NTA resin (Qiagen). The resin was washed by W1 buffer (25 mM Tris, pH 8.0, 500 mM NaCl) and W2 buffer (25 mM Tris, pH 8.0, 20 mM imidazole) and eluted by 25 mM Tris, pH 8.0, and 300 mM imidazole. The proteins were further purified by anion exchange chromatography (SOURCE 15Q, GE Healthcare).

Preparation of Sarcoplasmic Reticulum Membrane from Porcine Heart. The procedures for preparing the porcine sarcoplasmic reticulum membrane (SRM) were based on the previous study (46) with slight modifications. A single porcine heart cut into small pieces was resuspended in 5 volumes of homogenization buffer A (20 mM Hepes (2-[4-(2-hydroxyethyl)piperazin-1-yl]ethanesulfonic acid), pH 7.5, 150 mM NaCl, 5 mM EDTA, 1.3 μg/mL aprotinin; 1 μg/mL pepstatin; 5 μg/mL leupeptin; 0.2 mM phenylmethyl sulfonylfluoride [PMSF]). Homogenization was performed in a blender (JYL-C010, Joyoung) for 15 cycles. After removing the debris by low-speed centrifugation (6,000 × *g*) for 10 min, the supernatant was further centrifuged at high speed (20,000 × *g*) for 1 h. The pellet was resuspended in 2 volumes of homogenization buffer B (20 mM Hepes, pH 7.4; 1 M NaCl; 1.3 μg/mL

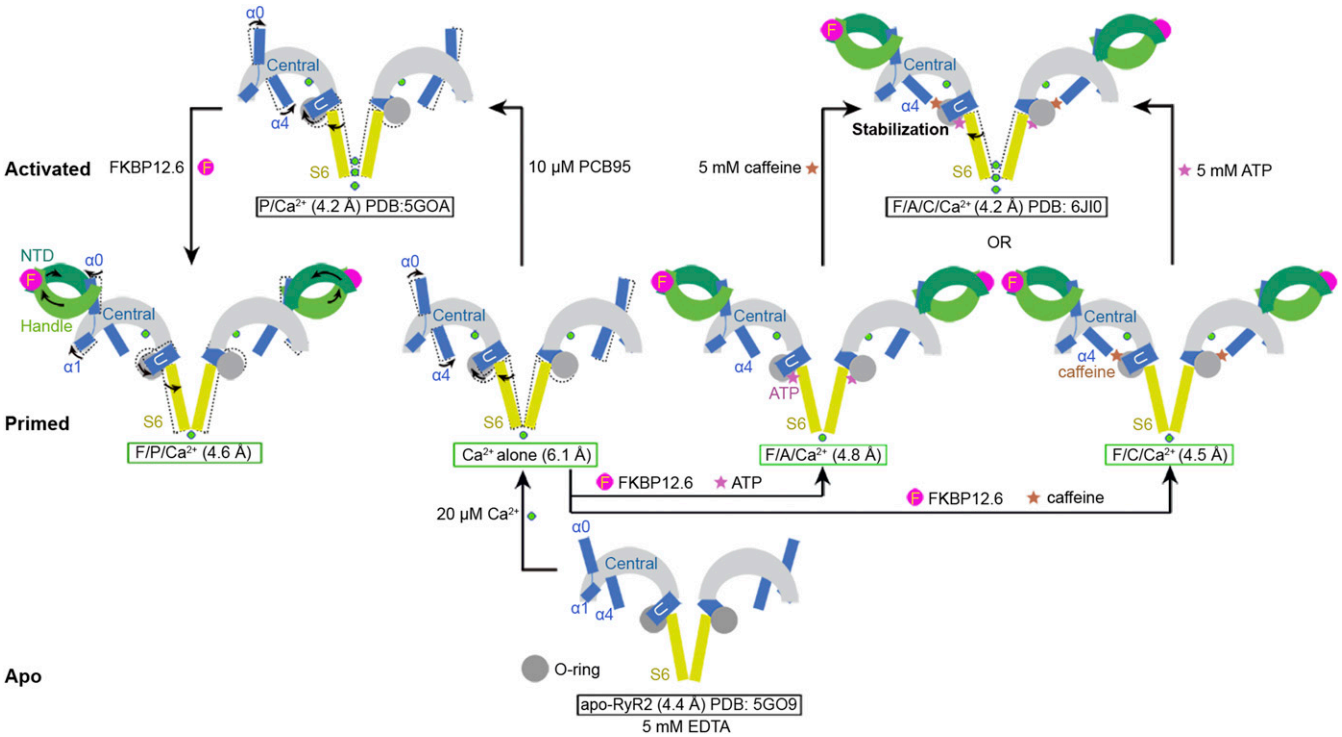

Fig. 4. Allosteric and concerted modulation of RyR2 by distinct factors. Shown here is a summary of the RyR2 structures reported in this (green box) and previous (black box) studies. Ca^{2+} alone induces a contraction of the central domain that provides a pulling force, facilitating the dilation of the S6 bundle. Addition of PCB95 induces further contraction of the central domain and opens the channel. FKBP12.6 induces a relaxation of the central domain, stabilizing RyR2 in a closed state. Caffeine locks the central domain in a constitutively contracted state, and ATP strengthens the effect of caffeine, stabilizing RyR2 in an open state in the presence of FKBP12.6.

aprotinin; 1 μg/mL pepstatin; 5 μg/mL leupeptin; 0.2 mM PMSF; and 2 mM dithiothreitol [DTT]) and flash frozen in liquid nitrogen.

Purification of pRyR2 by GST-FKBP12.6 and GST-FKBP12. The pRyR2/FKBP12.6 and pRyR2/FKBP12 complexes were purified by the same procedures according to a previous study (46) with slight modifications. The total SRM from a single heart was solubilized at 4 °C for 2 h in homogenization buffer B with 5% CHAPS and 1.25% soy bean lecithin. After extraction, the concentration of NaCl was diluted from 1 to 0.2 M by homogenization buffer lacking NaCl. Approximately 5 to 6 mg of GST-FKBP12.6 or GST-FKBP12 were then added to the system and incubated for 1 h. After ultrahigh-speed centrifugation (200,000 × *g*), the supernatant was loaded onto a GS4B column (GE Healthcare). The complex was eluted by a solution containing 80 mM Tris, pH 8.0, 200 mM NaCl, 10 mM GSH, 0.1% digitonin, 1.3 μg/mL aprotinin, 1 μg/mL pepstatin, 5 μg/mL leupeptin, 0.2 mM PMSF, and 2 mM DTT. The eluted protein was further purified through SEC (Superose 6, 10/300 GL, GE Healthcare) in buffer containing 20 mM Hepes, pH 7.4, 200 mM NaCl, 0.1% digitonin, 1.3 μg/mL aprotinin, 1 μg/mL pepstatin, 5 μg/mL leupeptin, 0.2 mM PMSF, and 2 mM DTT. The peak fractions were concentrated to ∼0.1 mg/mL for EM sample preparation. Other modulators were added to the samples before preparation of cryo-EM grids (*SI Appendix*, Table S1).

Cryo-EM Image Acquisition. Vitrobot Mark IV (FEI) was applied for preparation of cryo-EM grids. The procedures for preparing the 7 samples were same. Aliquots (3 μL each) of pRyR2 samples were placed on glow-discharged copper grids covered with continuous carbon film (Zhong jingkeyi Technology Co. Ltd.) or lacey carbon grids (Ted Pella Inc.). Grids were blotted for 2 s and flash frozen in liquid ethane. With regard to the Ca^{2+} alone, F/P/Ca^{2+}, and F/A/Ca^{2+} datasets, grids were then transferred to a Titan Krios (FEI) electron microscope equipped with a Gatan K2 Summit detector (Gatan Co.) and operated at 300 kV with a nominal magnification of 105,000×. The defocus value varied from −1.7 to −2.7 μm. Each stack was dose fractionated to 32 frames with a total electron dose of 48.6 $e^{-}/Å^2$ for a total exposure time of 8.0 s. The stacks were motion corrected with MotionCorr (65) and subjected to 2-fold binning, resulting in a pixel size of 1.30654 Å/pixel. With regard to the F/C/Ca^{2+} dataset, grids were then transferred to a Titan Krios electron microscope operating at 300 kV equipped with a Cs corrector (Thermo Fisher Scientific Inc.), Gatan K2 Summit detector, and GIF Quantum energy filter. The defocus value varied from −1.3 to −1.7 μm. Each stack was exposed in superresolution mode for 5.6 s with an exposure time of 0.175 s per frame, resulting in 32 frames per stack. The total dose was ∼50 $e^{-}/Å^2$ for each stack. The stacks were motion corrected with MotionCorr and subjected to 2-fold binning, resulting in a pixel size of 1.091 Å/pixel. For all of the datasets, the output stacks from MotionCorr were further motion corrected with MotionCor2 (66), and dose weighting was performed (67). The defocus values were estimated using Gctf (68).

Image Processing. Similar image processing procedures were employed as previously reported (46). Diagrams of the procedures used in data processing are presented in *SI Appendix*, Figs. S2 and S3. With regard to the reconstruction of F/P/Ca^{2+}, 543,280 particles were picked from 2,897 micrographs by RELION 2.0 (69) using low-pass-filtered templates to 20 Å to limit reference bias. After 2D classification, 215,884 particles were selected and subjected to global angular search 3D classification using RELION 2.0 with one class and step size of 7.5°. The EM map of the open structure P/Ca^{2+}, which was low pass filtered to 60 Å, was used as the initial model. After global angular search 3D classification, the particles were further subjected to 3D classification with 10 classes and a local angular search step of 3.75°. The local angular search 3D classification was performed several times with the output from different iterations of the global angular search 3D classification as input. After merging all good classes and removing the duplicated particles, the particles were subjected to 3D autorefinement. The final particle number for the 3D autorefinement was 60,287, thereby resulting in a 4.6 Å resolution map after postprocessing. The same procedures were performed for the other datasets. The resolution was estimated with the gold standard Fourier shell correlation 0.143 criterion (70) with the high-resolution noise substitution method (71).

Model Building and Structure Refinement. The model of RyR2 closed structure (Protein Data Bank [PDB] ID code 5GO9) (46) was fitted into the maps of the 4 conditions by Chimera (72) and manually adjusted in COOT (73). FKBP12 from the rRyR1 structure (PDB ID code 3J8H) (52) was used for homologous model building of FKBP12.6. Structure refinement was performed using PHENIX (74) in real space with restrained secondary structure and geometry. The statistics of the 3D reconstruction and model refinement are summarized in *SI Appendix*, Table S1.

Data Availability. Atomic coordinates and EM density maps of Ca^{2+} alone (PDB ID code 6JG3; EMDB ID code EMD-9823), F/P/Ca^{2+} (PDB ID code 6JGZ; EMDB ID code EMD-9824), F/A/Ca^{2+} (PDB ID code 6JH6; EMDB ID code EMD-9825), and F/C/Ca^{2+} (PDB ID code 6JHN; EMDB ID code EMD-9826) have been deposited in the PDB (http://www.rcsb.org) and the Electron Microscopy Data Bank (EMD) (https://www.ebi.ac.uk/pdbe/emdb/).

ACKNOWLEDGMENTS. We thank Xiaomin Li (Tsinghua University) for technical support during EM image acquisition. We thank the Tsinghua University Branch of the China National Center for Protein Sciences (Beijing) for providing the cryo-EM facility support. We are thankful for the computational facility support on the cluster of the Bio-Computing Platform (Tsinghua University Branch of the China National Center for Protein Sciences, Beijing) and the "Explorer 100" cluster system of Tsinghua National Laboratory for Information Science and Technology. This work was funded by the National Natural Science Foundation of China (projects 31621092, 31630017, 31930059, 81920108015, and 81861138009) and the National Key R&D Program (Grant 2016YFA0500402) and the National Key Basic Research (973) Program (Grant 2015CB910101) from the Ministry of Science and Technology of China. N.Y. is supported by the Shirley M. Tilghman endowed professorship from Princeton University.

1. I. N. Pessah, A. L. Waterhouse, J. E. Casida, The calcium-ryanodine receptor complex of skeletal and cardiac muscle. *Biochem. Biophys. Res. Commun.* **128**, 449–456 (1985).
2. E. F. Rogers *et al*., Plant insecticides; ryanodine, a new alkaloid from Ryania speciosa Vahl. *J. Am. Chem. Soc.* **70**, 3086–3088 (1948).
3. Z. Yuchi, F. Van Petegem, Ryanodine receptors under the magnifying lens: Insights and limitations of cryo-electron microscopy and X-ray crystallography studies. *Cell Calcium* **59**, 209–227 (2016).
4. D. M. Bers, Sarcoplasmic reticulum Ca release in intact ventricular myocytes. *Front. Biosci.* **7**, d1697–d1711 (2002).
5. M. Endo, Calcium release from the sarcoplasmic reticulum. *Physiol. Rev.* **57**, 71–108 (1977).
6. A. Fabiato, Calcium-induced release of calcium from the cardiac sarcoplasmic reticulum. *Am. J. Physiol.* **245**, C1–C14 (1983).
7. J. Nakai *et al*., Primary structure and functional expression from cDNA of the cardiac ryanodine receptor/calcium release channel. *FEBS Lett.* **271**, 169–177 (1990).
8. M. J. Berridge, Dysregulation of neural calcium signaling in Alzheimer disease, bipolar disorder and schizophrenia. *Prion* **7**, 2–13 (2013).
9. M. Fill, J. A. Copello, Ryanodine receptor calcium release channels. *Physiol. Rev.* **82**, 893–922 (2002).
10. C. H. George, H. Jundi, N. L. Thomas, D. L. Fry, F. A. Lai, Ryanodine receptors and ventricular arrhythmias: Emerging trends in mutations, mechanisms and therapies. *J. Mol. Cell. Cardiol.* **42**, 34–50 (2007).
11. P. J. Laitinen *et al*., Mutations of the cardiac ryanodine receptor (RyR2) gene in familial polymorphic ventricular tachycardia. *Circulation* **103**, 485–490 (2001).
12. A. Leenhardt, I. Denjoy, P. Guicheney, Catecholaminergic polymorphic ventricular tachycardia. *Circ. Arrhythm. Electrophysiol.* **5**, 1044–1052 (2012).
13. A. Medeiros-Domingo *et al*., The RYR2-encoded ryanodine receptor/calcium release channel in patients diagnosed previously with either catecholaminergic polymorphic ventricular tachycardia or genotype negative, exercise-induced long QT syndrome: A comprehensive open reading frame mutational analysis. *J. Am. Coll. Cardiol.* **54**, 2065–2074 (2009).
14. S. G. Priori, S. R. Chen, Inherited dysfunction of sarcoplasmic reticulum Ca2+ handling and arrhythmogenesis. *Circ. Res.* **108**, 871–883 (2011).
15. S. G. Priori *et al*., Clinical and molecular characterization of patients with catecholaminergic polymorphic ventricular tachycardia. *Circulation* **106**, 69–74 (2002).
16. S. G. Priori *et al*., Mutations in the cardiac ryanodine receptor gene (hRyR2) underlie catecholaminergic polymorphic ventricular tachycardia. *Circulation* **103**, 196–200 (2001).
17. D. R. Laver *et al*., Cytoplasmic Ca2+ inhibits the ryanodine receptor from cardiac muscle. *J. Membr. Biol.* **147**, 7–22 (1995).
18. G. Meissner, E. Darling, J. Eveleth, Kinetics of rapid Ca2+ release by sarcoplasmic reticulum. Effects of Ca2+, Mg2+, and adenine nucleotides. *Biochemistry* **25**, 236–244 (1986).
19. G. Meissner, J. S. Henderson, Rapid calcium release from cardiac sarcoplasmic reticulum vesicles is dependent on Ca2+ and is modulated by Mg2+, adenine nucleotide, and calmodulin. *J. Biol. Chem.* **262**, 3065–3073 (1987).
20. R. Sitsapesan, A. J. Williams, Gating of the native and purified cardiac SR Ca(2+)-release channel with monovalent cations as permeant species. *Biophys. J.* **67**, 1484–1494 (1994).
21. L. Xu, G. Mann, G. Meissner, Regulation of cardiac Ca2+ release channel (ryanodine receptor) by Ca2+, H+, Mg2+, and adenine nucleotides under normal and simulated ischemic conditions. *Circ. Res.* **79**, 1100–1109 (1996).

BIOCHEMISTRY

22. W. M. Chan, W. Welch, R. Sitsapesan, Structural factors that determine the ability of adenosine and related compounds to activate the cardiac ryanodine receptor. *Br. J. Pharmacol.* **130**, 1618–1626 (2000).
23. H. Kong *et al*., Caffeine induces Ca2+ release by reducing the threshold for luminal Ca2+ activation of the ryanodine receptor. *Biochem. J.* **414**, 441–452 (2008).
24. E. Rousseau, J. Ladine, Q. Y. Liu, G. Meissner, Activation of the Ca2+ release channel of skeletal muscle sarcoplasmic reticulum by caffeine and related compounds. *Arch. Biochem. Biophys.* **267**, 75–86 (1988).
25. G. L. Smith, S. C. O'Neill, A comparison of the effects of ATP and tetracaine on spontaneous Ca(2+) release from rat permeabilised cardiac myocytes. *J. Physiol.* **534**, 37–47 (2001).
26. L. H. Jeyakumar *et al*., FKBP binding characteristics of cardiac microsomes from diverse vertebrates. *Biochem. Biophys. Res. Commun.* **281**, 979–986 (2001).
27. S. O. Marx *et al*., PKA phosphorylation dissociates FKBP12.6 from the calcium release channel (ryanodine receptor): Defective regulation in failing hearts. *Cell* **101**, 365–376 (2000).
28. T. Seidler *et al*., Overexpression of FK-506 binding protein 12.0 modulates excitation contraction coupling in adult rabbit ventricular cardiomyocytes. *Circ. Res.* **101**, 1020–1029 (2007).
29. A. P. Timerman *et al*., The calcium release channel of sarcoplasmic reticulum is modulated by FK-506-binding protein. Dissociation and reconstitution of FKBP-12 to the calcium release channel of skeletal muscle sarcoplasmic reticulum. *J. Biol. Chem.* **268**, 22992–22999 (1993).
30. A. Tripathy, L. Xu, G. Mann, G. Meissner, Calmodulin activation and inhibition of skeletal muscle Ca2+ release channel (ryanodine receptor). *Biophys. J.* **69**, 106–119 (1995).
31. X. H. Wehrens *et al*., FKBP12.6 deficiency and defective calcium release channel (ryanodine receptor) function linked to exercise-induced sudden cardiac death. *Cell* **113**, 829–840 (2003).
32. L. Xu, A. Tripathy, D. A. Pasek, G. Meissner, Potential for pharmacology of ryanodine receptor/calcium release channels. *Ann. N. Y. Acad. Sci.* **853**, 130–148 (1998).
33. A. B. Brillantes *et al*., Stabilization of calcium release channel (ryanodine receptor) function by FK506-binding protein. *Cell* **77**, 513–523 (1994).
34. X. H. Wehrens *et al*., Protection from cardiac arrhythmia through ryanodine receptor-stabilizing protein calstabin2. *Science* **304**, 292–296 (2004).
35. S. Barg, J. A. Copello, S. Fleischer, Different interactions of cardiac and skeletal muscle ryanodine receptors with FK-506 binding protein isoforms. *Am. J. Physiol.* **272**, C1726–C1733 (1997).
36. D. L. Sackett, D. Kosk-Kosicka, The active species of plasma membrane Ca2+-ATPase are a dimer and a monomer-calmodulin complex. *J. Biol. Chem.* **271**, 9987–9991 (1996).
37. E. Galfré *et al*., FKBP12 activates the cardiac ryanodine receptor Ca2+-release channel and is antagonised by FKBP12.6. *PLoS One* **7**, e31956 (2012).
38. J. Z. Zhang *et al*., FKBPs facilitate the termination of spontaneous Ca2+ release in wild-type RyR2 but not CPVT mutant RyR2. *Biochem. J.* **473**, 2049–2060 (2016).
39. R. H. Ashley, A. J. Williams, Divalent cation activation and inhibition of single calcium release channels from sheep cardiac sarcoplasmic reticulum. *J. Gen. Physiol.* **95**, 981–1005 (1990).
40. A. Zahradníková, I. Zahradník, Description of modal gating of the cardiac calcium release channel in planar lipid membranes. *Biophys. J.* **69**, 1780–1788 (1995).
41. M. T. Alonso *et al*., Ca2+-induced Ca2+ release in chromaffin cells seen from inside the ER with targeted aequorin. *J. Cell Biol.* **144**, 241–254 (1999).
42. A. Herrmann-Frank, H. C. Lüttgau, D. G. Stephenson, Caffeine and excitation-contraction coupling in skeletal muscle: A stimulating story. *J. Muscle Res. Cell Motil.* **20**, 223–237 (1999).
43. M. Samsó, W. Feng, I. N. Pessah, P. D. Allen, Coordinated movement of cytoplasmic and transmembrane domains of RyR1 upon gating. *PLoS Biol.* **7**, e85 (2009).
44. P. W. Wong, I. N. Pessah, Noncoplanar PCB 95 alters microsomal calcium transport by an immunophilin FKBP12-dependent mechanism. *Mol. Pharmacol.* **51**, 693–702 (1997).
45. P. W. Wong, I. N. Pessah, Ortho-substituted polychlorinated biphenyls alter calcium regulation by a ryanodine receptor-mediated mechanism: Structural specificity toward skeletal- and cardiac-type microsomal calcium release channels. *Mol. Pharmacol.* **49**, 740–751 (1996).
46. W. Peng *et al*., Structural basis for the gating mechanism of the type 2 ryanodine receptor RyR2. *Science* **354**, aah5324 (2016).
47. D. Gong *et al*., Modulation of cardiac ryanodine receptor 2 by calmodulin. *Nature* **572**, 347–351 (2019).
48. A. des Georges *et al*., Structural basis for gating and activation of RyR1. *Cell* **167**, 145–157.e17 (2016).
49. K. Willegems, R. G. Efremov, Influence of lipid mimetics on gating of ryanodine receptor. *Structure* **26**, 1303–1313.e4 (2018).
50. N. Paknejad, R. K. Hite, Structural basis for the regulation of inositol trisphosphate receptors by Ca^{2+} and IP_3. *Nat. Struct. Mol. Biol.* **25**, 660–668 (2018).
51. X. C. Bai, Z. Yan, J. Wu, Z. Li, N. Yan, The central domain of RyR1 is the transducer for long-range allosteric gating of channel opening. *Cell Res.* **26**, 995–1006 (2016).
52. Z. Yan *et al*., Structure of the rabbit ryanodine receptor RyR1 at near-atomic resolution. *Nature* **517**, 50–55 (2015).
53. L. Kimlicka, K. Lau, C. C. Tung, F. Van Petegem, Disease mutations in the ryanodine receptor N-terminal region couple to a mobile intersubunit interface. *Nat. Commun.* **4**, 1506 (2013).
54. P. W. Wong, E. F. Garcia, I. N. Pessah, ortho-Substituted PCB95 alters intracellular calcium signaling and causes cellular acidification in PC12 cells by an immunophilin-dependent mechanism. *J. Neurochem.* **76**, 450–463 (2001).
55. S. Dhindwal *et al*., A cryo-EM-based model of phosphorylation- and FKBP12.6-mediated allosterism of the cardiac ryanodine receptor. *Sci. Signal.* **10**, eaai8842 (2017).
56. A. P. Timerman *et al*., Selective binding of FKBP12.6 by the cardiac ryanodine receptor. *J. Biol. Chem.* **271**, 20385–20391 (1996).
57. T. Guo *et al*., Kinetics of FKBP12.6 binding to ryanodine receptors in permeabilized cardiac myocytes and effects on Ca sparks. *Circ. Res.* **106**, 1743–1752 (2010).
58. G. P. Ahern, P. R. Junankar, A. F. Dulhunty, Ryanodine receptors from rabbit skeletal muscle are reversibly activated by rapamycin. *Neurosci. Lett.* **225**, 81–84 (1997).
59. G. P. Ahern *et al*., Effects of ivermectin and midecamycin on ryanodine receptors and the Ca2+-ATPase in sarcoplasmic reticulum of rabbit and rat skeletal muscle. *J. Physiol.* **514**, 313–326 (1999).
60. L. A. Gonano, P. P. Jones, FK506-binding proteins 12 and 12.6 (FKBPs) as regulators of cardiac ryanodine receptors: Insights from new functional and structural knowledge. *Channels (Austin)* **11**, 415–425 (2017).
61. C. C. Deivanayagam, M. Carson, A. Thotakura, S. V. Narayana, R. S. Chodavarapu, Structure of FKBP12.6 in complex with rapamycin. *Acta Crystallogr. D Biol. Crystallogr.* **56**, 266–271 (2000).
62. H. B. Xin, K. Rogers, Y. Qi, T. Kanematsu, S. Fleischer, Three amino acid residues determine selective binding of FK506-binding protein 12.6 to the cardiac ryanodine receptor. *J. Biol. Chem.* **274**, 15315–15319 (1999).
63. Z. Yuchi, K. Lau, F. Van Petegem, Disease mutations in the ryanodine receptor central region: Crystal structures of a phosphorylation hot spot domain. *Structure* **20**, 1201–1211 (2012).
64. O. Haji-Ghassemi, Z. Yuchi, F. Van Petegem, The cardiac ryanodine receptor phosphorylation hotspot embraces PKA in a phosphorylation-dependent manner. *Mol. Cell* **75**, 39–52.e4 (2019).
65. X. Li *et al*., Electron counting and beam-induced motion correction enable near-atomic-resolution single-particle cryo-EM. *Nat. Methods* **10**, 584–590 (2013).
66. S. Q. Zheng *et al*., MotionCor2: Anisotropic correction of beam-induced motion for improved cryo-electron microscopy. *Nat. Methods* **14**, 331–332 (2017).
67. T. Grant, N. Grigorieff, Measuring the optimal exposure for single particle cryo-EM using a 2.6 Å reconstruction of rotavirus VP6. *eLife* **4**, e06980 (2015).
68. K. Zhang, Gctf: Real-time CTF determination and correction. *J. Struct. Biol.* **193**, 1–12 (2016).
69. D. Kimanius, B. O. Forsberg, S. H. Scheres, E. Lindahl, Accelerated cryo-EM structure determination with parallelisation using GPUs in RELION-2. *eLife* **5**, e18722 (2016).
70. P. B. Rosenthal, R. Henderson, Optimal determination of particle orientation, absolute hand, and contrast loss in single-particle electron cryomicroscopy. *J. Mol. Biol.* **333**, 721–745 (2003).
71. S. Chen *et al*., High-resolution noise substitution to measure overfitting and validate resolution in 3D structure determination by single particle electron cryomicroscopy. *Ultramicroscopy* **135**, 24–35 (2013).
72. E. F. Pettersen *et al*., UCSF Chimera–A visualization system for exploratory research and analysis. *J. Comput. Chem.* **25**, 1605–1612 (2004).
73. P. Emsley, B. Lohkamp, W. G. Scott, K. Cowtan, Features and development of coot. *Acta Crystallogr. D Biol. Crystallogr.* **66**, 486–501 (2010).
74. P. D. Adams *et al*., PHENIX: A comprehensive Python-based system for macromolecular structure solution. *Acta Crystallogr. D Biol. Crystallogr.* **66**, 213–221 (2010).